This is the author's version of an article that has been published in this journal. Changes were made to this version by the publisher prior to publication.
The final version of record is available at http://dx.doi.org/10.1109/TAP.2019.2949417

Orientation-Insensitive and Normalization-Free Reading Chipless RFID system based on Circular Polarization Interrogation

Simone Genovesi, *Member, IEEE*, Filippo Costa, *Member, IEEE*, Francesco Alessio Dicandia, Michele Borgese, and Giuliano Manara, *Fellow, IEEE*

***Abstract*—A novel normalization-free reading scheme to recover data encoded in chipless RFID tags is presented. The proposed approach exploits the circular polarization to isolate the field scattered by the tag from that of surrounding objects. The desired polarization mismatch is achieved by exploiting the properties of high-impedance surfaces that can suitably manipulate the reflected field. A thorough analysis of the interaction between the circularly polarized interrogation and the field scattered by the chipless RFID tag as well as the hosting platform is provided. The proposed method does not require any a-priori calibration if a reading antenna with a suitable axial ratio is available. More importantly, the CP-based reading approach guarantees the correct tag detection regardless of the tag orientation. The case of the tag mounted on metallic platform is also analyzed and it is demonstrated that the circular polarization reading procedure is robust under the hypothesis of a proper axial ratio of the probing antennas. The minimum requirements of axial ratio are derived by using a theoretical model. Measurements confirmed the speculations obtained through the theoretical analysis both in the case of low-scattering items as well as for metallic platforms.**

***Index Terms* — Chipless RFID, circular polarization, Radio Frequency IDentification (RFID), mounted on metal tag, normalization free.**

I. Introduction

CHIPLESS Radio Frequency IDentification (RFID) has recently attracted the attention of the scientific community that has proposed several approaches for designing a tag that does not require an integrated circuit to encode information. Basically, the reader interrogates with a stimulus (*e.g.* electromagnetic wave) the passive tag that reflects a certain amount of the impinging power depending on the Radar Cross Section (RCS) of the chipless tag, the reader gain and their relative distance with the advantage that no energy is spent to activate the chip as in the case of standard RFID [1], [2]. Essentially, the information encoded in the tag is stored into the backscattered frequency or time domain response by exploiting different schemes. In particular, amplitude modulation [3], phase quantization [4], [5], frequency shifts [6], [7], time delays and hybrid approaches mixing some of the aforementioned quantities [8]–[10] are exploited to embed the information into the scattered field collected by the reader. However, for chipless RFID systems that are not near-field or contactless [11], major challenges remain to be tackled in order to improve the overall performance and applicability in real-life scenarios. In particular, the antenna employed by the reader does not collect only the scattering from the chipless tag but also comprises contributions from the field reflected by nearby objects (Fig. 1). These unwanted signals clearly affect the correct retrieving of the encoded data. In order to mitigate this problem, several approaches relying on dual polarization interrogation [12], cross-polarization exploitation [13], [14] or signal processing techniques have been investigated [15]. The solutions based on copolar interrogation usually struggle if the chipless RFID tag is placed on a metallic object since the scattering of the tag can be overwhelmed by the strong electromagnetic echo of the hosting platform. Techniques based on depolarizing tags [13] [14] are more efficient in isolating the tag contribution but they usually require a particular relative orientation between the tag and the transmitter/reader antennas in order to maximize the probability of correct detection. A few studies focusing on the possibility to obtain both a good tag isolation from the surrounding environment and insensitivity to polarization are available. In [16] a system employing two dual-polarized antennas, RF switches, a 4-port vector network analyzer (VNA) and the short-time Fourier transform (STFT) analysis is presented. However, this approach has not been tested when the tag is placed on metallic objects. In [17] a circularly-polarized chipless tag with a short delay line is employed in a UWB reading system. The transmitting and receiving antenna are respectively linearly and orthogonally polarized to reduce the antenna coupling. Consequently, the receiver collects only a fraction of the field scattered by the tag due to polarization mismatch, and the reading process depends on the tag orientation. A single measurement of the transmission coefficient magnitude between two antennas in front of a tag has been proved to be successful in [18] as far as the transmission coefficient between the antennas in presence of

Simone Genovesi, Filippo Costa and Giuliano Manara are with Dipartimento di Ingegneria dell'Informazione, University of Pisa, Pisa 56122, Italy (www.dii.unipi.it). (e-mail: simone.genovesi, filippo.costa, giuliano.manara [@unipi.it]).

Francesco Alessio Dicandia and Michele Borgese were with Dipartimento di Ingegneria dell'Informazione, University of Pisa. (e-mail: alessio.dicandia, michele.borgese [@for.unipi.it]).

Work partially supported by the Italian Ministry of Education and Research (MIUR) in the framework of the CrossLab project (Departments of Excellence).

Copyright (c) 2019 IEEE. Personal use is permitted. For any other purposes, permission must be obtained from the IEEE by emailing pubs-permissions@ieee.org.

This is the author's version of an article that has been published in this journal. Changes were made to this version by the publisher prior to publication.
The final version of record is available at http://dx.doi.org/10.1109/TAP.2019.2949417

the tag exhibits a much greater magnitude than the coupling between the antenna in absence of the tag.

This paper proposes a class of chipless RFID tags that can be read regardless of its orientation, and even when placed on a metallic object, by exploiting the properties of circular polarization (CP) probing and properly designing the chipless RFID tags. The features that the tag must exhibit are defined in Section II whereas the importance of the contribution of both copolar and cross-polar component of the reflected field to the overall scattering is remarked in Section III. Section IV analyzes the effects of the finite cross-polar discrimination on the noise introduced in the collected signal at the receiver. Characterization of the reading system in terms of axial ratio of the employed circular-polarized antennas and performance of the new reading paradigm on low-scattering objects are assessed with measurements in Section V. Section VI addresses the reading of chipless RFID tag placed on highly scattering platforms and final conclusions are provided in Section VII.

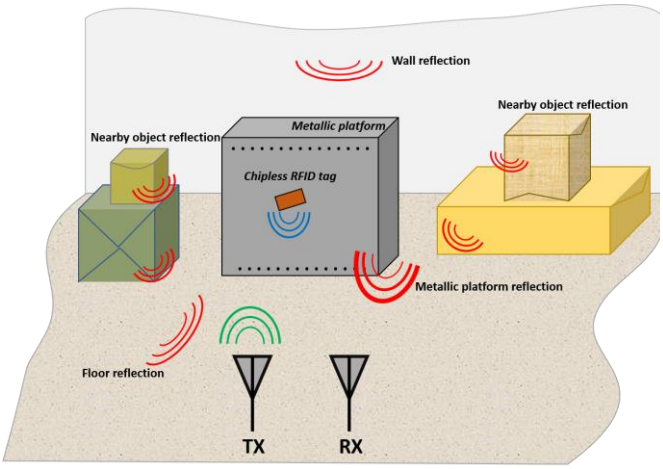

Fig. 1. Example of operative scenario: the transmitter (TX) probes the chipless RFID tag and the receiver (RX) collects strong reflections from the metallic platform, echoes from nearby objects, multipath contributions and the coupling with the TX.

II. Reflection of Circular Polarization on an HIS

Let us consider a right-handed circularly polarized (RHCP) plane wave generated by a RHCP antenna propagating in air along +z direction that impinges on a planar interface. The incident field $\underline{E}^{inc}$ can be written as [19]:

$$\underline{E}^{inc} = E_0\,\underline{i}_x + jE_0\,\underline{i}_y \tag{1}$$

where $\underline{i}_x$ and $\underline{i}_y$ are the unit vectors along x-axis and y-axis, respectively, and E_0 represents the magnitude of each component. The reflected electric field $\underline{E}^{ref}$ can be expressed as:

$$\begin{aligned}\underline{E}^{ref} &= \left(\Gamma_{xx}E_0 + j\Gamma_{xy}E_0\right)\underline{i}_x + \left(\Gamma_{yx}E_0 + j\Gamma_{yy}E_0\right)\underline{i}_y = \\ &= \underline{E}_x^{ref}\,\underline{i}_x + \underline{E}_y^{ref}\,\underline{i}_y\end{aligned} \tag{2}$$

where Γ_{xx} and Γ_{yy} are the copolar reflection coefficients whereas Γ_{xy} and Γ_{yx} are the cross-polar ones. In case the interface is between air and a perfect electric conducting (PEC) surface, $\Gamma_{xx} = \Gamma_{yy} = -1$ and $\Gamma_{xy} = \Gamma_{xy} = 0$ and the polarization of the wave remains purely CP but its handedness is changed. Therefore, a receiving antenna will see the incoming reflected wave as:

$$\underline{E}^{ref} = -E_0\,\underline{i}_x - jE_0\,\underline{i}_y \tag{3}$$

which can be fully collected with a properly circularly-polarized (CP) antenna that maximizes the Polarization Loss Factor (*PLF*) defined as:

$$PLF = \left|\underline{\rho}_{ref}\cdot\underline{\rho}_{RX}\right|^2 \tag{4}$$

where ρ_{ref} is the polarization vector of the reflected wave and ρ_{RX} is the polarization vector of the CP receiving antenna, which is defined by the polarization vector of the wave it transmits. Therefore, considering that:

$$\underline{\rho}_{ref} = \frac{\underline{E}_x^{ref}\,\underline{i}_x + \underline{E}_y^{ref}\,\underline{i}_y}{\left|\underline{E}^{ref}\right|},\quad \underline{\rho}_{RX}^{RH/LH} = \frac{1}{\sqrt{2}}\left(\underline{i}_x \pm j\underline{i}_y\right) \tag{5}$$

it can be found that the PLF for the reflected wave defined in (3), that is the PEC case, achieves its maximum unitary value if a left-handed (LH) CP antenna is employed at the receiver side. On the contrary, the PLF will be zero. Let us consider a case in which the two copolar components of the CP plane wave experience different reflections and the cross-polar components are temporarily neglected. In particular, if $\Gamma_{xx} = 1$, $\Gamma_{yy} = -1$ and $\Gamma_{xy} = \Gamma_{yx} = 0$, it can be easily seen that the PLF is maximized to 1 only if a right-handed (RH) CP antenna is adopted at the receiver side since:

$$\underline{E}^{ref} = E_0\,\underline{i}_x - jE_0\,\underline{i}_y,\quad \underline{\rho}_{RX}^{RH} = \frac{1}{\sqrt{2}}\left(\underline{i}_x + j\underline{i}_y\right) \tag{6}$$

More in detail, the result found in (6) is typical of any interface that reflects the two copolar components with same magnitude but a phase difference of 180°.The aforementioned condition can be satisfied by a High-Impedance Surface (HIS) [20], although only at some frequencies and not within a continuous bandwidth [21]. The necessary condition is the same needed for a linear reflection polarization converter [22], [23]. An example of this behavior is reported for two different HISs, realized with periodic surfaces [24] printed on a grounded dielectric slab ($\varepsilon_r = 2.8$, tg δ =0.03 and thickness = 1.524 mm). The unit cell of the periodic surface of dimensions T_x and T_y is discretized into a 32 x 32 pixel matrix and analyzed with a Periodic Method of Moments (PMoM) [25]. The former unit cell comprises a dipole (Fig. 2a) whereas the latter has a loop (Fig. 2b).

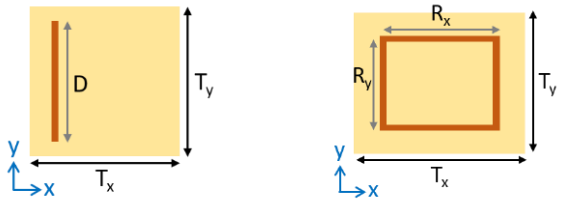

(a) *(b)*

Fig. 2. Two different HIS unit cells: single dipole *(a)* and single ring *(b)*.

The copolar phase response of each HIS is shown in Fig. 3 for a normal incident plane wave. The periodicities along both planar directions (*x*, *y*) have been set to obtain a resonance frequency around 2.4 GHz for both HISs, namely $T_x = T_y = 4.2$ cm for the dipole and $T_x = 2.3$ cm, $T_y = 1.9$ cm for

Copyright (c) 2019 IEEE. Personal use is permitted. For any other purposes, permission must be obtained from the IEEE by emailing pubs-permissions@ieee.org.

This is the author's version of an article that has been published in this journal. Changes were made to this version by the publisher prior to publication.
The final version of record is available at http://dx.doi.org/10.1109/TAP.2019.2949417

the ring. The other dimensions are D = 3.94 cm, R_x = 2.15cm and R_y = 1.78 cm. It is apparent that the phase difference, *delta*, between TE and TM polarization is equal to 180° for a single frequency in the case of the dipole (Fig. 3a) whereas it is obtained twice within the interval 2.4 GHz-2.6 GHz for the ring (Fig. 3b).

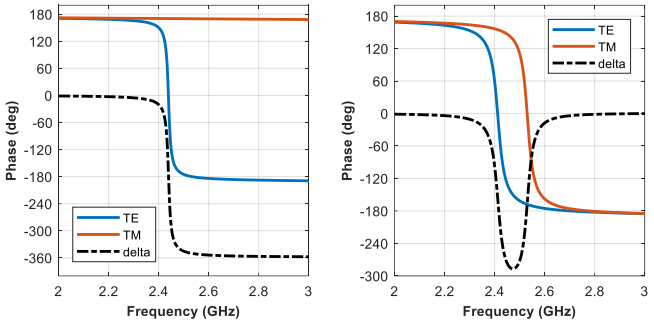

(a) *(b)*

Fig. 3. Phase response of the two HISs: single dipole *(a)* and single ring *(b)*.

III. Cross-polar contribution to the Scattered Field for Chipless Tag Reading independent of Tag Orientation

Before considering the PLFs of the two HISs as a function of their orientation with respect to the incident field, let us analyze the importance of the cross-polar contribution to the reflected field. In particular, the aim is to observe the differences in the field scattered by the two considered HISs in order to provide some useful hints for the choice of the most promising HIS candidate for the chipless RFID tag. The analysis considers the orthogonal incidence ($\theta = 0°$with respect to z-axis) of plane waves for different values of ϕ (with respect to x-axis).

First of all, it is apparent from Fig. 4 that taking into account only the copolar components of the reflected electric field, an incorrect magnitude of the reflection coefficient is obtained.

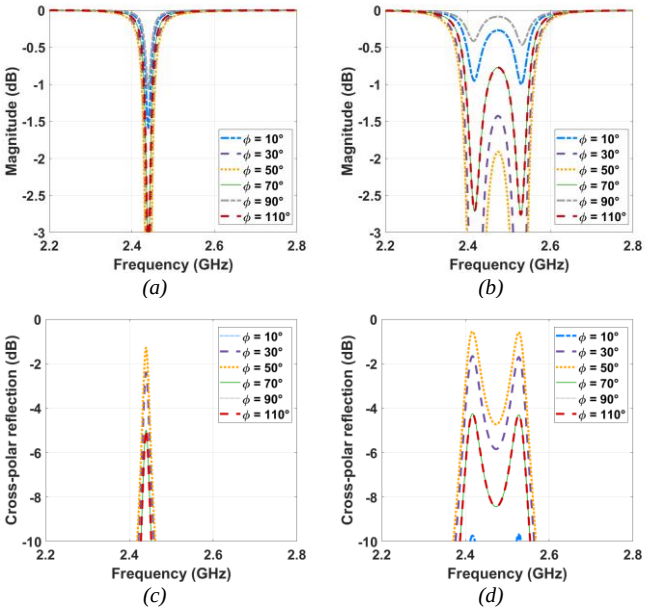

(a) *(b)* *(c)* *(d)*

Fig. 4. Copolar magnitude of the electric field reflected by the dipole-based HIS *(a)* and ring-based HIS *(b)*. Cross-polar magnitude of the cross-polar reflection coefficient: dipole-based HIS *(c)* and ring-based HIS *(d)*.

Indeed, the reflected field significantly depends on the angle ϕ. For the azimuth angle ϕ=*0,* there is no depolarization effect of the dipole and the cross-polar component of the reflection coefficient, Γ_{xy}, is negligible. However, when the electric field is not aligned with the dipole, the depolarizing effect the dipole plays an important role and the cross-polar reflection coefficient cannot be neglected. In the case of the ring shaped periodic surface, it is evident the there are two minima since the loop is rectangular [26]. This is the consequence of the fact that the 180° phase difference condition is encountered twice for each resonance as highlighted in Fig. 3. The contribution of the cross-polar component to the scattered field is illustrated in where the ring-based HIS always provides a higher level of cross-polar reflection. The frequency response is stable also for an oblique incidence up to θ = 30° although a spurious peak appears starting from θ = 20° out of the considered bandwidth around 5.6 GHz.

The magnitude of the total scattered field is finally shown in Fig. 5 where two important conclusions can be drawn. The former is that the cross-polar contribution must be taken into account since the difference in the evaluation of the reflected electric field can be in the order of 2 dB or even more (*e.g.* Fig.4 and Fig. 5a). The latter is that the ring-based HIS exhibits a higher level of the reflected field in correspondence of the frequencies where the phase difference is equal to 180°since the losses introduced by the ring are lower than those of the dipole [27]. It is also worthwhile to observe that the response is stable with respect to angle ϕ (Fig. 5) for both cases. Due to the lower losses, the ring-based HIS seems a better candidate for the design of chipless RFID tags and therefore a multi-ring version of it has been investigated in the next section to assess the performance of the CP for recovering the information stored on arbitrary-oriented tags. However, if the spectral bit capacitance is the major concern, the best choice is the dipole-based HIS since it allows a higher density of resonant elements and closer resonant peaks within the considered bandwidth.

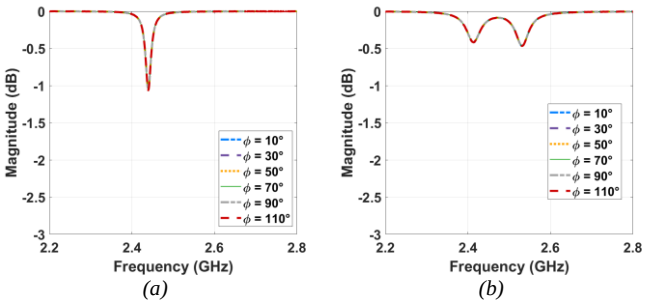

(a) *(b)*

Fig. 5. Magnitude of the total electric field reflected by the dipole-based HIS *(a)* and ring-based HIS *(b)* including the cross-polar contribution.

The multi-ring tag is reported in Fig. 6, together with a table summarizing the periodicity of the HIS and each ring dimension in terms of the 32 x 32 pixel matrix adopted by the PMoM.

Each ring is able to provide the necessary 180° phase difference between the two components of the reflected field in two closely-spaced frequencies, regardless of the value assumed by ϕ as shown in Fig. 7. More in detail, *Ring#1* achieves this condition in two frequencies around 2.45 GHz (*i.e.* 2.4 GHz, 2.52 GHz), *Ring#2* close to 3.55 GHz (*i.e.*

Copyright (c) 2019 IEEE. Personal use is permitted. For any other purposes, permission must be obtained from the IEEE by emailing pubs-permissions@ieee.org.

This is the author's version of an article that has been published in this journal. Changes were made to this version by the publisher prior to publication.
The final version of record is available at http://dx.doi.org/10.1109/TAP.2019.2949417

3.49 GHz, 3.62 GHz) and *Ring#3* near 4.85 GHz (4.77 GHz, 4.98 GHz). It is also important to highlight that these frequencies do not shift with respect to ϕ incidence angle.

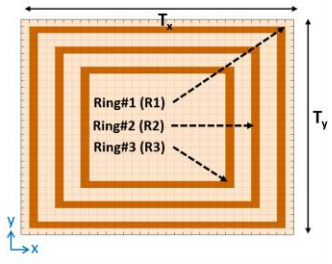

T_x	2.3cm (32 pixel)
T_y	1.9cm (32 pixel)
$R1_x$	30 pixel
$R1_y$	30 pixel
$R2_x$	24 pixel
$R2_y$	24 pixel
$R3_x$	18 pixel
$R3_y$	18 pixel

Fig. 6. Unit cell comprising three rings whose periodicity and dimensions are reported in the table.

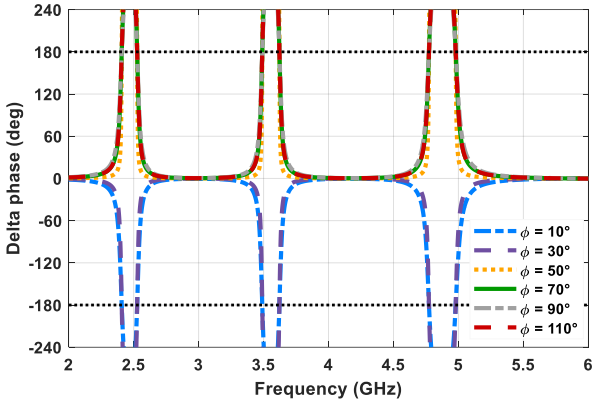

Fig. 7. Phase difference *delta* for different values of angle of incidence ϕ ($\theta = 0°$) of the investigated three-ring HIS.

Let us now consider a transmitting antenna radiating a RHCP plane wave impinging on a PEC surface. The PLF evaluated for a LHCP and RHCP receiving antenna is maximized to 1 in the whole bandwidth by the former choice whereas it is equal to 0 for the latter, as expected. On the contrary, if the transmitted plane wave probes the designed HIS (Fig. 6), the PLF is maximized only in correspondence of the aforementioned frequency couples by a RHCP receiving antenna (Fig. 8), as predicted by the analysis carried out in Section II. This is particularly appealing since the field scattered from a metallic platform is polarization-mismatched with a RCHP antenna. In addition, the electric field reflected from surrounding objects and multipath contributions do not fully match as the one reflected by a chipless RFID tag exploiting the described HIS.

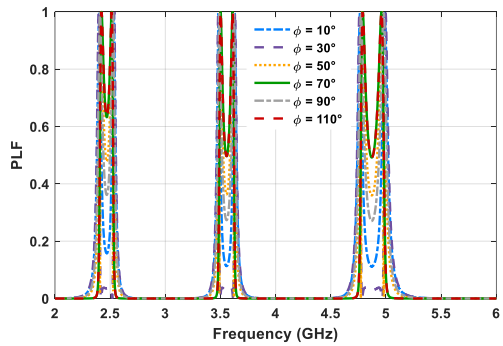

Fig. 8. PLF in case of a CP plane wave impinging upon the considered HIS surface. The transmitter is a RHCP antenna and the receiver is a RHCP antenna

IV. Effects of Finite Cross Polar Discrimination

In the analysis reported in Section II the considered incident field in (1) exhibits only a RHCP plane wave. However, it is important to consider that the cross polar discrimination (XPD) of a real antenna, defined as the ratio between the magnitude of the copolar field and the cross-polar one (*i.e.* XPD = $|E_{RHCP}|/|E_{LHCP}|$), is not ideal (XPD$\rightarrow\infty$) and it has a finite value. Therefore, the interrogating field will have both CP handedness, although only one is obviously dominant.

Let us consider the electric field radiated by the probing antenna, $\underline{E}^{inc}$, as the superposition of a RHCP and a LHCP plane wave [19]:

$$\underline{E}^{inc} = \underline{E}^{inc\,(RH)} + \underline{E}^{inc\,(LH)} \tag{7}$$

where the RHCP is considered the *primary* wave whereas the LHCP the *secondary* contribution. The magnitude of the impinging electric field is therefore:

$$\left|E^{inc}\right| = \left|E^{inc(RH)}\right|\left(1+\frac{1}{XPD}\right) \tag{8}$$

Once the RHCP incident wave impinges on the chipless RFID tag mounted on an object, the reflected electric field, $\underline{E}^{ref}$, can be written as the superposition of four contributions:

$$\underline{E}^{ref} = \underline{E}_{tag}^{ref\,(RH)} + \underline{E}_{tag}^{ref\,(LH)} + \underline{E}_{obj}^{ref\,(LH)} + \underline{E}_{obj}^{ref\,(RH)} \tag{9}$$

where the first two terms refer to the chipless RFID tag scattering and the last two to the reflection caused by the hosting platform. In case of antennas radiating/receiving only the RHCP plane wave (i.*e.* infinite XPD), the reflected field comprises only the RH scattered wave from the tag and the LH wave of the object. Therefore, the collected signal is only RHCP polarized since the receiving antenna is totally mismatched to the LHCP, thanks to the hypothesized infinite XPD.

In a real scenario (i.*e.* finite XPD), all the four scattering contributions have to be carefully considered. More in particular, we could have two different cases, namely, when the tag is placed on weakly-scattering objects, such as cardboard or plastic boxes, and when it is collocated on a metallic platform. In both cases, we can reasonably assume that the hosting object is made of a homogenous and isotropic material and therefore $\Gamma_{xx} = \Gamma_{yy} = M\exp(j\mu)$ and $\Gamma_{xy} = \Gamma_{xy} = 0$, with $|M| < 1$ and $\mu \in [0,2\pi)$ in the former case and $|M| = 1$ and $\mu = \pi$ in the latter one.

Let us consider the previously mentioned case in which the antenna mainly transmits a RHCP plane wave. The amplitude of the undesired CP plane wave (*i.e.* LHCP one) can be easily expressed as a function of the RH one by using the XPD. Subsequently, if we assume that the RH component of the radiated field exhibits a power density $S_{RH} = S$ then the LHCP component has $S_{LH} = S / XPD^2$. The transmitted power density impinges upon the chipless RFID tag and the hosting object, with a radar cross section equal to σ_{tag} and σ_{obj}, respectively.

Copyright (c) 2019 IEEE. Personal use is permitted. For any other purposes, permission must be obtained from the IEEE by emailing pubs-permissions@ieee.org.

This is the author's version of an article that has been published in this journal. Changes were made to this version by the publisher prior to publication.
The final version of record is available at http://dx.doi.org/10.1109/TAP.2019.2949417

The total power P_{tot} that is collected by the receiving antenna in correspondence of the resonance frequencies of the HIS is then proportional to:

$$P_{tot} \propto S\sigma_{tag} + \frac{S}{XPD^2}\sigma_{obj} + \frac{S}{XPD^4}\sigma_{tag} + \frac{S}{XPD^2}\sigma_{obj} \approx S\sigma_{tag} + 2\frac{S}{XPD^2}\sigma_{obj} \quad (10)$$

where we have not considered the effect of the distance between the antennas and the tagged object.

The first term ($S\sigma_{tag}$) represents the power associated to the information we want to decode. In fact, the RHCP plane wave impinges upon the tag and it is reflected as a RCHP one in correspondence of the HIS resonances. This RH contribution is then fully collected by the polarization-matched receiving antenna. The second term is the RHCP plane wave that is reflected as a LHCP one by the object and then it is affected by a finite polarization mismatch when collected at the receiver. It is important to remark that outside the HIS resonances, the chipless RFID tag behaves like a PEC object as well. The third term is the LHCP plane wave that is reflected as a LHCP one by the tag and then is mismatched at the receiver side (this term is negligible since the tag RCS is low and it is scaled for the power of four of XPD). The last term is the LHCP plane wave that impinges upon the object, where its polarization is reversed, and it is then fully collected by the receiving antenna. The first term is the only one we are interested to collect, which must be greater than the sum of all the others that represent just noise. The power associated with this term has to emerge from the noise floor of a certain quantity that is sufficient to be correctly retrieved by the adopted receiver. The next section will analyze the results of measurements in operative environment on the basis of this analysis to assess the overall performance of the proposed reading paradigm.

V. Measurements on Low-Scattering Objects

In Section III, the frequency response and the PLF have been calculated by considering infinite surfaces (PEC or HIS) and their interaction with CP plane waves. In order to assess the performance of the proposed detection paradigm, a finite chipless RFID tag has been fabricated and tested in a non-anechoic environment. In order to have a CP probing, two dual-polarized horns (Flann DP240-AB) have been fed as described in Fig. 9a.

More in detail, a 90-degree hybrid coupler (DQ-DJ-2080 from A-INFO) has been used to provide the necessary phase difference between the two antenna ports in order to generate a CP wave. The other two ports of the hybrid have been connected to the vector network analyzer, VNA, (Keysight - E5071C) and to a matched load, respectively. The output power of the VNA was set equal to 0 dBm.

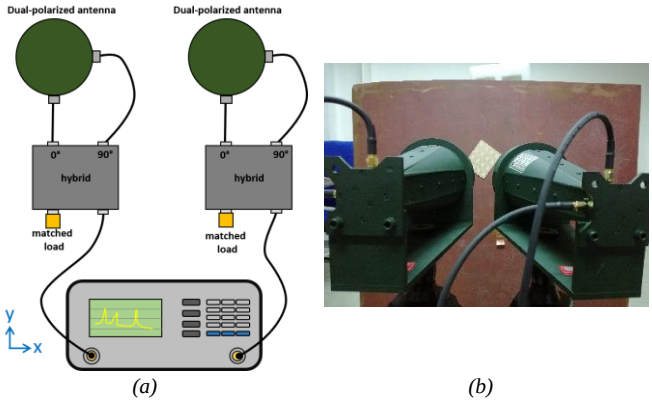

(a) (b)

Fig. 9. Measurement setup: VNA connections to the hybrids and feeding scheme for the dual-polarized horns *(a)*, reading of the randomly-oriented chipless RFID tag on the metal platform *(b)*.

The achieved Axial Ratio (AR) and the Cross-Polar Discrimination (XPD) factor for the RHCP one are illustrated in Fig. 10, respectively. The degree of circular polarization achieved with the described antenna setup is rather good for the two highest frequencies (1.5 dB and 2.1 dB), but it is barely acceptable for the lowest one as it is apparent from the AR shown in Fig. 10. The XPD is higher than 20 dB for the highest frequency and around 20 dB on average for the intermediated one. However, the lowest peak suffers of a small frequency region where the XPD is close to 15 dB and this could cause a degradation of the decoding performance. A 4x4 chipless RFID tag, whose overall area is around 70 cm^2, has been fabricated as well (Fig. 11).

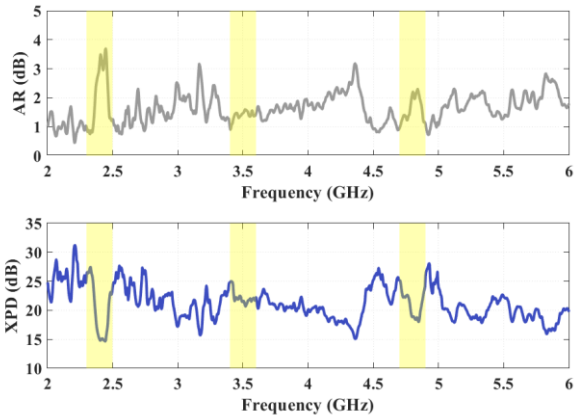

Fig. 10. Axial ratio of the RHCP plane wave generated by the described antenna setup and cross-polar discrimination of the employed antenna. Frequency bandwidths of interest are emphasized in light yellow.

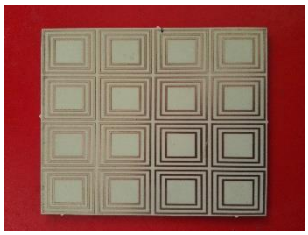

Fig. 11. Fabricated 4x4 chipless RFID tag for testing on a metal platform and in a non-anechoic environment.

Copyright (c) 2019 IEEE. Personal use is permitted. For any other purposes, permission must be obtained from the IEEE by emailing pubs-permissions@ieee.org.

This is the author's version of an article that has been published in this journal. Changes were made to this version by the publisher prior to publication.
The final version of record is available at http://dx.doi.org/10.1109/TAP.2019.2949417

The chipless RFID tag has been placed on cardboard boxes or Teflon packages and the distance between the antennas and the tag was 40 cm. A reading of this measurement configuration is reported in Fig. 12 in which are compared the case with and without the chipless RFID tag. The agreement between measurements and simulations is quite satisfactory since the peaks of the reflected wave are within the expected frequency interval and also exhibit the typical "twice" peak of the rectangular-ring HIS. The sharp behavior of the PLF seen in the simulations (see Section III) is not apparent in the trend of the collected signal at the receiving antenna but this was expected due to the non-ideal circularly-polarized plane wave generated and to the finite XPD of the receiving antenna as addressed in the previous section. It is worth mentioning that no background subtraction has been performed.

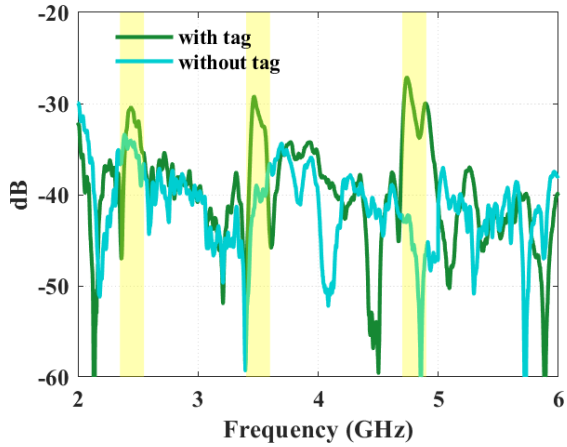

Fig. 12. Signal collected (S_{21}) when the chipless RFID is on cardboard (no metallic surface). Frequency bandwidths of interest are highlighted in light yellow. The distance between the tag and the reading antenna is 40 cm.

Before testing the chipless RFID on a metal platform it is worthwhile to consider again the total received power (10) and analyze the differences between the case in which the tag is placed on a low-scattering platform (*e.g.* cardboard, Teflon) or on a strong-scattering one (*e.g.* PEC). In particular, for the XPD measured in correspondence of the HIS, it can be reasonably assumed that the third term, which is proportional to σ_{tag} / XPD^4, can be neglected. The total received power can then be approximated as proportional to:

$$P_{tot} \propto S\sigma_{tag} + 2\frac{S}{XPD^2}\sigma_{obj} \qquad (11)$$

For a successful reading it is therefore required that at the HIS resonances:

$$S\,\sigma_{tag} > 2\frac{S}{XPD^2}\sigma_{obj} \qquad (12)$$

that states that the collected power associated to the information content has to be greater than the noise to be successfully decoded. If we consider the case of container, made of 3 mm-thick Teflon, where the chipless RFID tag is placed on one 1sqm-area face, it is possible to estimate the two different power values. In particular, it is important to focus on the difference between the power associated to the information and that of the noise in correspondence of the resonances of the chipless RFID tag. More in detail, the comparison between the power associated to the information and the noise is illustrated in Fig. 13. The curves are obtained by firstly evaluating the reflected field $\underline{E}^{ref}$ as described in (2) and (9) for both circular polarizations by considering the measured XPD of the employed transmitting antenna (Fig. 10) and the theoretical reflection coefficient of a 3 mm-thick Teflon slab or the chipless tag. Next the correspondent received power for each component of the reflected field is calculated by using the power density of the reflected field ($\underline{S}^{ref}$), the simulated RCS of the tag or the Teflon object, the distance R between the antenna and the tag, the effective area of the receiving antenna (A_{eff}) and the XPD in case of polarization mismatch:

$$\mathrm{P_r} = S^{ref}\sigma_{tag/obj}\left(\frac{1}{4\pi R^2}\right)A_{eff}\,\frac{1}{XPD^2}\,. \qquad (13)$$

It is apparent that for an impinging power density S upon the tag placed on the square Teflon platform of 1 sqm area, the power associated to the info exceeds the noise component more than 5dBmW on average. It is apparent that the proposed chipless RFID tag provides good performance in this scenario since guarantees a high intelligibility of the information. It is worthwhile to mention that, as stated in (10), if the probing antennas would exhibit a better AR, thus a larger XPD, the difference would be even larger.

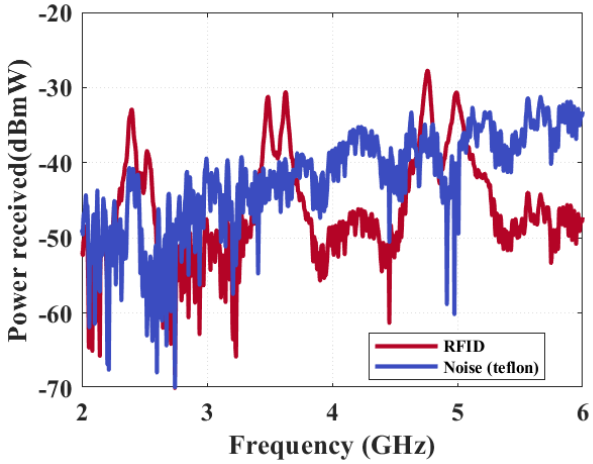

Fig. 13. Comparison of power associated to information and noise in case the chipless RFID tag is placed on a square Teflon surface of 1 sqm area. Distance between antennas and Teflon surface is 40 cm.

VI. Assessment on Metallic Hosting Platforms

The placement of the proposed chipless RFID tag on a metallic object presents additional challenges. In fact, as already mentioned, a non-ideal AR of the probing antennas can cause an undesired scattering contribution of the hosting platform that in this case can completely overwhelm the

Copyright (c) 2019 IEEE. Personal use is permitted. For any other purposes, permission must be obtained from the IEEE by emailing pubs-permissions@ieee.org.

This is the author's version of an article that has been published in this journal. Changes were made to this version by the publisher prior to publication.
The final version of record is available at http://dx.doi.org/10.1109/TAP.2019.2949417

information encoded in the field scattered by the chipless RFID tag. The dimensions of the metallic object with respect to the chipless RFID tag is another important issue. As an example, let us consider a square PEC platform of side equal to 25cm hosting the 4x4 chipless RFID tag that is interrogated with a normally-impinging plane wave with the measured XPD obtained with the realized setup (Fig. 10). The comparison between the theoretical power, obtained as in (12), associated to the useful information and to the noise is reported in Fig. 14.

The power associated to the noise is comparable with the one of the information. It is important to observe that the area of the PEC platform is roughly 9 times that of the 4x4 chipless RFID tag. Removing the power density and explicating the RCS, the relation (12) can be reformulated as:

$$A_{tag}^2 > 2\frac{A_{obj}^2}{XPD^2}. \quad (14)$$

If M is defined as the ratio between the area of the tag and that of the hosting metallic object, $M = A_{obj} / A_{tag}$, we finally obtain that the value of XPD necessary for having the received power associated to the information content greater than the noise on is expressed as:

$$XPD > \sqrt{2}M \quad (15)$$

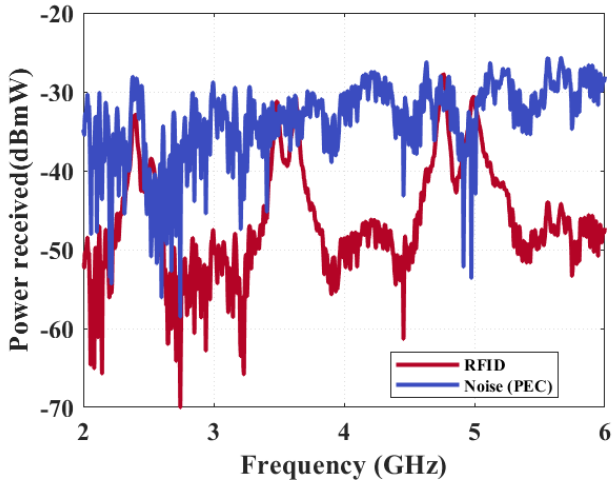

Fig. 14. Comparison of power associated to information and noise in case the chipless RFID tag is placed on a square PEC surface (side = 25 cm)

The comparison between the employed XPD and different values of area ratio M is illustrated in Fig. 15. It is apparent that the adopted system can cope with M up to 3 but for greater ratios it is necessary to improve the XPD, especially for the lowest frequency peak. Measurements of the 4x4 chipless RFID placed on a square PEC platform of 3 times its area are shown in Fig. 16 and assesses the expected successful reading. It has also to be remarked that the considered theoretical speculations case is somewhat a worst one since we are considering a perfectly planar surface. For example, in case the tag is attached on a cargo container whose surface are undulated for increasing mechanical robustness, the reflected power is diffused on a larger volume and less focused, thus favoring a decrease on the noise collected at the receiver. This scattering diffusion effect of an undulated or the scattering deflection of non-planar metallic surface could improve the detection range of the tag with respect to the wort case defined according to relation (13). Obviously, increasing the size of the tag (e.g. 5x5 or 6x6) will improve the overall performance at no further design cost, since the enhancement of the chipless RCS is obtained by adding the same unit cell. The resulting improvement of the system reliability will also cause a lower spatial bit density.

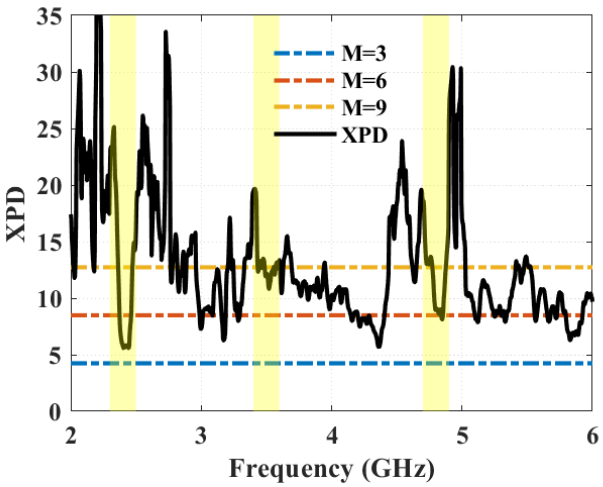

Fig. 15. Comparison between the XPD of the employed antennas and different values of M (ratio between the area of the hosting metallic object and the chipless RFID tag). Frequency bandwidths of interest are highlighted in light yellow.

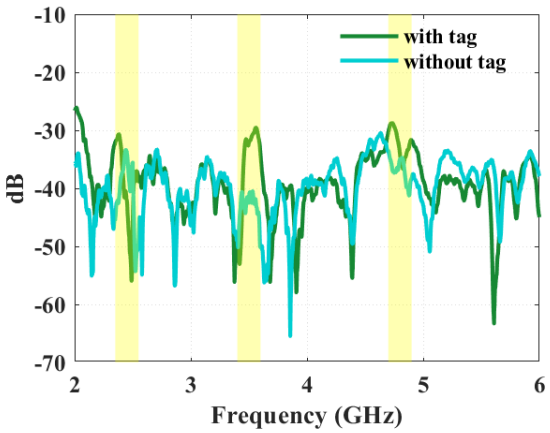

Fig. 16. Signal collected by the receiver antenna for a chipless RFID placed on 25 cm x 25 cm metallic plate. Frequency bandwidths of interest are highlighted in light yellow.

VII. Conclusions

A novel Chipless RFID reading scheme exploiting the advantageous properties of the circular polarization has been proposed. The information embedded into the tag is recovered from the field scattered by a depolarizing CP tag by discriminating the handedness of the received signal. The necessary conditions that the field reflected by the tag must

Copyright (c) 2019 IEEE. Personal use is permitted. For any other purposes, permission must be obtained from the IEEE by emailing pubs-permissions@ieee.org.

This is the author's version of an article that has been published in this journal. Changes were made to this version by the publisher prior to publication.
The final version of record is available at http://dx.doi.org/10.1109/TAP.2019.2949417

satisfy have been described and design criteria have been suggested by resorting to the properties of high-impedance surfaces. An important benefit of the adopted approach consists in reading the tag independently from its orientation with respect to the incident field. The proposed reading scheme allows the rejection of the contribution from objects near the tag thanks to the polarization diversity. Consequently, the tag detection can be carried out without any normalization procedure provided that the polarization discrimination characteristic of the reader antenna satisfies the minimum requirement theoretically defined in the paper. A careful analysis for both weak-scattering and strong-scattering hosting platform has been carried out and useful relations between the *XPD* of the employed reader and dimension of the hosting platform with respect to the chipless RFID tag have been provided. The performance of the proposed technique has been assessed with measurements on a fabricated prototype that proved a satisfactory agreement with estimated results.

REFERENCES

[1] K. V. S. Rao, P. V. Nikitin, K. V. S. Rao, and P. V. Nikitin, "Theory and measurement of backscattering from RFID tags," *IEEE Antennas Propag. Mag.*, vol. 48, no. 6, pp. 212–218, Dec. 2006.

[2] A. T. Blischak and M. Manteghi, "Embedded Singularity Chipless RFID Tags," *IEEE Trans. Antennas Propag.*, vol. 59, no. 11, pp. 3961–3968, Nov. 2011.

[3] F. Costa, S. Genovesi, and A. Monorchio, "A Chipless RFID Based on Multiresonant High-Impedance Surfaces," *IEEE Trans. Microw. Theory Tech.*, vol. 61, no. 1, pp. 146–153, Jan. 2013.

[4] I. Balbin and N. C. Karmakar, "Phase-Encoded Chipless RFID Transponder for Large-Scale Low-Cost Applications," *IEEE Microw. Wirel. Compon. Lett.*, vol. 19, no. 8, pp. 509–511, Aug. 2009.

[5] S. Genovesi, F. Costa, A. Monorchio, and G. Manara, "Chipless RFID tag exploiting multifrequency delta-phase quantization encoding," *IEEE Antennas Wirel. Propag. Lett.*, vol. 15, pp. 738–741, 2016.

[6] A. Vena, E. Perret, and S. Tedjini, "High-Capacity Chipless RFID Tag Insensitive to the Polarization," *IEEE Trans. Antennas Propag.*, vol. 60, no. 10, pp. 4509–4515, Oct. 2012.

[7] C. M. Nijas *et al.*, "Low-Cost Multiple-Bit Encoded Chipless RFID Tag Using Stepped Impedance Resonator," *IEEE Trans. Antennas Propag.*, vol. 62, no. 9, pp. 4762–4770, Sep. 2014.

[8] A. Vena, E. Perret, and S. Tedjini, "Chipless RFID Tag Using Hybrid Coding Technique," *IEEE Trans. Microw. Theory Tech.*, vol. 59, no. 12, pp. 3356–3364, Dec. 2011.

[9] S. Tedjini, N. Karmakar, E. Perret, A. Vena, R. Koswatta, and R. E-Azim, "Hold the Chips: Chipless Technology, an Alternative Technique for RFID," *IEEE Microw. Mag.*, vol. 14, no. 5, pp. 56–65, Jul. 2013.

[10] F. Costa, S. Genovesi, A. Monorchio, and G. Manara, "A Robust Differential-Amplitude Codification for Chipless RFID," *IEEE Microw. Wirel. Compon. Lett.*, vol. 25, no. 12, pp. 832–834, Dec. 2015.

[11] C. Herrojo, J. Mata-Contreras, F. Paredes, and F. Martín, "Microwave Encoders for Chipless RFID and Angular Velocity Sensors Based on S-Shaped Split Ring Resonators," *IEEE Sens. J.*, vol. 17, no. 15, pp. 4805–4813, Aug. 2017.

[12] F. Costa, S. Genovesi, and A. Monorchio, "Normalization-Free Chipless RFIDs by Using Dual-Polarized Interrogation," *IEEE Trans. Microw. Theory Tech.*, vol. 64, no. 1, pp. 310–318, Gennaio 2016.

[13] F. Costa, S. Genovesi, and A. Monorchio, "Chipless RFIDs for Metallic Objects by Using Cross Polarization Encoding," *IEEE Trans. Antennas Propag.*, vol. 62, no. 8, pp. 4402–4407, Aug. 2014.

[14] S. Preradovic, I. Balbin, N. C. Karmakar, and G. F. Swiegers, "Multiresonator-Based Chipless RFID System for Low-Cost Item Tracking," *IEEE Trans. Microw. Theory Tech.*, vol. 57, no. 5, pp. 1411–1419, May 2009.

[15] A. Ramos, E. Perret, O. Rance, S. Tedjini, A. Lazaro, and D. Girbau, "Temporal Separation Detection for Chipless Depolarizing Frequency-Coded RFID," *IEEE Trans. Microw. Theory Tech.*, vol. 64, no. 7, pp. 2326–2337, Jul. 2016.

[16] M. Garbati, E. Perret, R. Siragusa, and C. Halopè, "Toward Chipless RFID Reading Systems Independent of Tag Orientation," *IEEE Microw. Wirel. Compon. Lett.*, vol. 27, no. 12, pp. 1158–1160, Dec. 2017.

[17] Y. Shen and C. L. Law, "A Low-Cost UWB-RFID System Utilizing Compact Circularly Polarized Chipless Tags," *IEEE Antennas Wirel. Propag. Lett.*, vol. 11, pp. 1382–1385, 2012.

[18] J. Kracek, M. Svanda, and K. Hoffmann, "Scalar Method for Reading of Chipless RFID Tags Based on Limited Ground Plane Backed Dipole Resonator Array," *IEEE Trans. Microw. Theory Tech.*, vol. 67, no. 11, Nov. 2019.

[19] C. A. Balanis, *Antenna Theory: Analysis and Design*, 4 edition. Hoboken, New Jersey: Wiley, 2016.

[20] D. Sievenpiper, L. Zhang, R. F. J. Broas, N. G. Alexopolous, and E. Yablonovitch, "High-impedance electromagnetic surfaces with a forbidden frequency band," *IEEE Trans. Microw. Theory Tech.*, vol. 47, no. 11, pp. 2059–2074, Nov. 1999.

[21] F. Costa, S. Genovesi, and A. Monorchio, "On the Bandwidth of High-Impedance Frequency Selective Surfaces," *IEEE Antennas Wirel. Propag. Lett.*, vol. 8, pp. 1341–1344, 2009.

[22] M. Borgese, F. Costa, S. Genovesi, A. Monorchio, and G. Manara, "Optimal Design of Miniaturized Reflecting Metasurfaces for Ultra - Wideband and Angularly Stable Polarization Conversion," *Sci. Rep.*, vol. 8, no. 1, p. 7651, May 2018.

[23] S. Genovesi, F. Costa, M. Borgese, F. A. Dicandia, and G. Manara, "Chipless Radio Frequency Identification (RFID) Sensor for Angular Rotation Monitoring," *Technologies*, vol. 6, no. 3, p. 61, Sep. 2018.

[24] R. Mittra, C. H. Chan, and T. Cwik, "Techniques for analyzing frequency selective surfaces-a review," *Proc. IEEE*, vol. 76, no. 12, pp. 1593–1615, Dec. 1988.

[25] S. Genovesi, A. Monorchio, R. Mittra, and G. Manara, "A Sub-boundary Approach for Enhanced Particle Swarm Optimization and Its Application to the Design of Artificial Magnetic Conductors," *IEEE Trans. Antennas Propag.*, vol. 55, no. 3, pp. 766–770, Mar. 2007.

[26] B. Munk, *Frequency selective surfaces: theory and design*. New York: John Wiley, 2000.

[27] F. Costa and A. Monorchio, "Closed-Form Analysis of Reflection Losses in Microstrip Reflectarray Antennas," *IEEE Trans. Antennas Propag.*, vol. 60, no. 10, pp. 4650–4660, Oct. 2012.

Copyright (c) 2019 IEEE. Personal use is permitted. For any other purposes, permission must be obtained from the IEEE by emailing pubs-permissions@ieee.org.